Design and Implementation of a Novel Robot Fish with Active and Compliant Propulsion Mechanism

Yong Zhong and Ruxu Du
Institute of Precision Engineering, Dept. of Mechanical and Automation Engineering
The Chinese University of Hong Kong, {yzhong, rdu}@mae.cuhk.edu.hk

Abstract — **Although methods about building fish-like robots have attracted much research in recent years, new techniques are still required for developing superior robot fish. This paper presents a novel robot fish propelled by an active compliant propulsion mechanism. The key innovation is the combination of an active wire-driven mechanism with a soft compliant tail to accomplish subcarangiform swimming (i.e., swimming with an "S" motion). Additionally, an effective design methodology based on a 3R pseudo-rigid-body model is proposed to design the compliant tail. First, the mathematical model based on the design methodology was derived and computer simulations were performed. Second, a prototype was fabricated and numerous experimental studies were conducted. The experiments demonstrated that the predictions of the mathematical model matched the testing results. Compared with existing robot fishes which use multi-link structure with each joint being actuated by one motor, the new robot fish has several advantages: it is simple in structure, easy to control, and capable of high speed swimming and maneuverable swimming, the maximum swimming speed reached 2.15 body length per second and the instantaneous maximum turning speed is 269°/s. Furthermore, the design methodology presented in the paper can be also used in other applications such as flexible probe of medical devices and soft manipulators.**

I. Introduction

In the search for more effective underwater propulsion methods, fish-like robot, or simply called robot fish, have attracted considerable research attention in recent 20 years. According to the literature, the most common design of the robot fish is the multi-link design or hyper-redundant manipulator design, in which each joint being actuated by a motor [1–4]. However, this type of design is marred by its complex structure and control as well as low energy efficiency, because about 80% of mechanical efficiencies is consumed through frictional losses and actuator losses [5]. The other prevalent design involves using smart materials, such as shape memory alloy, through which the actuation is obtained by changing the temperature [6–7]; and ionic polymer metal composite actuator, through which the actuation is obtained by applying electrical stimulation [8–9]. The smart-material-based design is simple and compact in size, but its efficiency is low when converting electrical energy into kinetic energy. Clearly, finding a simple and efficient propulsion system is highly valuable.

In nature, many creatures, such as fish, snake, and some worms, have a flexible and soft body. These creatures particularly adapt to complex environments, such as underwater, trees and complex terrain. Inspired by these creatures, a number of soft robot fish have been built. Such robots offer advantages including easy fabrication, easy control, and high stability in locomotion. For example, Alvarado et al has developed a couple of robot fishes with compliant bodies [10-11]. C. Fiazza et al [12] developed similar robot fish and test different materials. The compliant bodies were fabricated using soft elastic materials. The actuation was conducted by vibrating the body at its natural frequency, namely, reaching the resonance frequency, then the entire body underwent an undulation motion. Therefore, a small stimulus could generate high and lasting propulsion and high swimming efficiency. They reported that the performance of their robot fishes were highly similar to that of the real fish, despite the considerable errors in the targeted kinematics. Daou et al [13] built a robot fish with a compliant body and proposed a model to take into account the inhomogeneous distribution of material along the compliant body and the effects of attaching a rigid caudal fin at the end. Feilich et al [14] fabricated passive fish caudal fins to determine the effects of shape and stiffness on the propulsion. Kopman et al [15] reported a similar approach. However, these existing complaint constructed robot fishes can flap only with specific patterns or modes because of their simple structure. For example, they are hard to perform a quick turning motion, and when the actuation frequency is different from the natural frequencies of the compliant system, the efficiency of such robot fishes would be considerable reduced. Therefore, using total compliant/passive tail to build a robot fish will diminish the controllability and maneuverability of the system due to few active controlled degree of freedoms. Additionally, to ensure that these robot fishes can swimming in undulatory motion (i.e., flapping in "S" shape), they must be actuated at a second resonance frequency [13], which is often too high for fish swimming mechanism. It shall be mentioned that while the oscillatory swimming is powerful, it is less efficient than undulatory swimming because "S" motion can transmit the travelling wave move efficient in the water and it is more stable in swimming [16].

Beyond the kinematics motion limits, the design and modelling art in [10, 13] were based on Bernoulli-Euler beam equation. From a mathematical perspective, a compliant tail can be modeled according to the Bernoulli–Euler beam equation if the bending amplitude is relatively small, but when the bending is high, it becomes nonlinear and the Bernoulli–Euler beam equation is not applicable. In consequence, the kinematics error is relatively large in [10]. To solve nonlinear beam issue, many mathematicians, scientists, and engineers have developed methodologies which might be crudely categorized as either analytical or based on *finite element* techniques [17–20]. However, these methods suffer from either difficulties in solving nonlinear differential equations or long time consumption to compute numerical solution. Other than these methods, Howell [21] proposed a linear model called pseudo-rigid-body model, which is composed of rigid body links and torsional springs, to analyze systems that undergo large, nonlinear deflections. This

simple model was usually used to the preliminary design of compliant mechanism and was proved to be effective [22]. In our study, we developed a methodology to design the compliant tail of robot fish based on pseudo-rigid-body model.

As mentioned previously, total compliant/passive tail constructed method diminish the control and maneuverable performance of the robot fish; therefore we need to develop a new type of propulsion mechanism. This motivated us to design and build a new type of robot fish that can achieve undulatory swimming at relatively high speed and simultaneously own high maneuverability. In previous work, a series of robot fishes based on the wire/cable-driven mechanism [23–26] were developed, for example, reference [25] developed a robot fish propelled by two-segment wire/cable-driven mechanism, which was actuated by two motors, and can achieve undulatory swimming and oscillatory swimming. However, in [25], two-segment wire/cable-driven mechanism have 13 joints, on which the friction may cause significant energy lost. To remedy this problem, the new robot fish is based on a combination of the wire-driven mechanism and the compliant tail. This combination can achieve undulatory motion and highly maneuverable motion using just one motor, and exerted a superior swimming performance. It achieved a maximum swimming speed of 2.15 BL/s (body length per second). Totally, it greatly improved the performance of robot fish.

The rest of this paper is organized as follows. Section 2 presents the design methodology. Section 3 presents the simulation and model analysis. The prototype fabrication and experimental results are presented in Section 4. Finally, Section 5 highlights the contributions and future work.

II. DESIGN OF THE ROBOT FISH

The new robot fish consists of three parts: head, active body (i.e., wire-driven mechanism) and complaint tail as shown in Fig. 1(a). The head, equipped with a pair of mechanical pectoral fins, hosts the control electronics, battery, servomotors, and driving reel. The design of the *active compliant propulsion mechanism* (ACPM), which contains the active body and complaint tail, are detailed as follows:

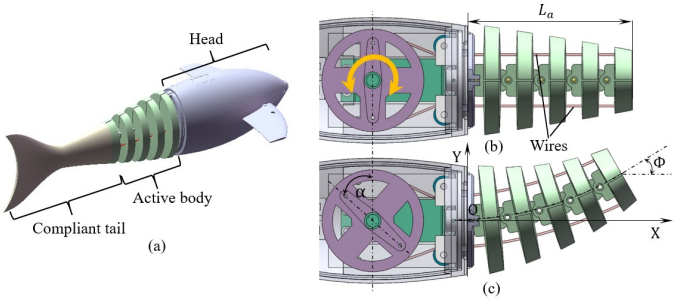

Figure 1. Robot fish overview (a) and the design of the active body.(b) is the initial status and (c) is the bending status.

A. Active body

The design of the active body is presented in Fig. 1(b) and (c). The coordinate system X'O'Y' is set at the center of the connecting plate between the head and active body. It moves when the robot fish moves (i.e., it is a function of time). As shown in Fig. 1(b), the active body is composed of five vertebras driven by a pair of inextensible wires, and its total length is L_a. In addition, the wires are driven by a servomotor through a reel. When the servomotor rotates, one wire contracts, whereas the other wire stretches, causing the active body to bend into an arc (Fig. 1(c)). This is a "C" motion in which the rotation angle α of the servomotor corresponds to the bending angle Φ of the active body:

$$\mathcal{R}: \alpha(t) \to \Phi(t) \tag{1}$$

This relationship is determined by the design parameters of the active body. Under ideal conditions (i.e., when the friction of each joint is the same), the rotation angles of every joint are identical (Fig. 2). Moreover, the length, H, of each vertebra is the same, and the gap, h_0, between the vertebras is the same. The two wires are parallel and the distance between them is d.

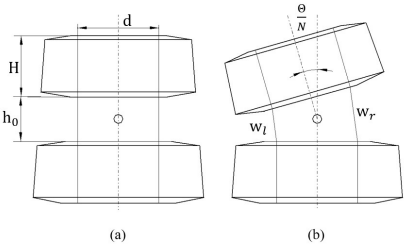

Figure 2. A concise illustration of every two vertebras

When a joint rotates, the length of the wire changes according to the following formulae:

$$\begin{cases} \Delta w_l = -\left[d \sin\left(\dfrac{\Phi}{2N}\right) + 2h_0 \sin^2\left(\dfrac{\Phi}{4N}\right)\right] \\ \Delta w_r = d \sin\left(\dfrac{\Phi}{2N}\right) - 2h_0 \sin^2\left(\dfrac{\Phi}{4N}\right) \end{cases} \tag{2}$$

where, N is the number of joints, and the subscripts l and r refer to the left and right sides, respectively. The rotation angle of each joint is Φ/N; because this value is relatively small, the *quadratic terms* can be ignored. Therefore, the relationship can be written as:

$$\Delta w_r = -\Delta w_l = d \sin(\frac{\Phi}{2N}). \tag{3}$$

The total change in the wire is controlled by the rotation of the reel. Therefore, the mapping relationship can be represented as:

$$\alpha = \frac{180}{\pi r} Nd \sin\left(\frac{\Phi}{2N}\right). \tag{4}$$

The position of every joint in the active body in the coordinate system X'O'Y' is given by

$$\begin{cases} x_i(t) = \sum_{j=1}^{i} \left((H + h_0) \cos\left(\dfrac{i\Phi}{N}\right)\right) \\ y_i(t) = \sum_{j=1}^{i} \left((H + h_0) \sin\left(\dfrac{i\Phi}{N}\right)\right) \end{cases}, \tag{5}$$

where $x_i(t)$ and $y_i(t)$ denote the coordinates of the i^{th} joint of the active body; by using this equation, the midline curve of the active body can be calculated.

B. Compliant Tail

The compliant tail, which is mounted on the last vertebra of the active body, is made of soft material. When the active body bends, it lags behind causing the robot fish to flap in an "S" shape motion (undulation). The model of the complaint tail is illustrated in Fig. 3.

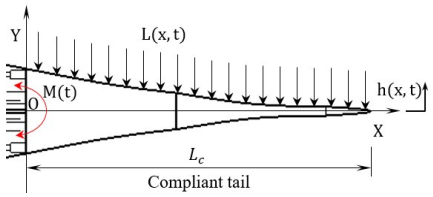

Figure 3. An illustration of the compliant tail under distributed forces.

As shown in Fig. 3, the compliant tail undergoes an external load and then it can deform. When the robot fish swims, the reaction force of water functions as the external load. In other words, the deflection of the compliant tail is determined not only by the stiffness of the compliant tail, but also by the external load. For simplicity, a coordinate system XOY is set at the origin of the compliant tail. The external forces acting on the compliant tail are the hydrodynamic forces, $L(x,t)$. The moment $M(t)$ of the compliant tail is generated by the active body. Moreover, $h(x, t)$ denotes the lateral deflection, and L_c is the length of the compliant tail. The distributed hydrodynamic force $L(x,t)$ per unit length for an inviscid steady flow is considered perpendicular to the compliant body midline and is expressed as [27]:

$$L(x,t) = m(x)\left(\frac{\partial^2 h}{\partial t^2} + 2U\frac{\partial^2 h}{\partial x \partial t} + U^2\frac{\partial^2 h}{\partial x^2}\right) \tag{6}$$

where U is the cursing speed, h is the lateral displacement of the compliant tail, and $m(x) = 0.25\pi S_c^2 \rho\tau$ is the effective added mass per unit length at the length x, S_c is the width of the tail at the length x, ρ is the fluid density and τ is a non-dimensional parameter close to 1.

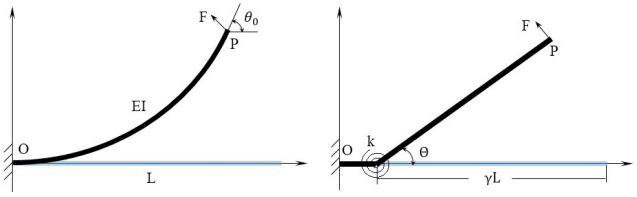

Figure 4. Illustration of (a) a cantilevered segment with forces at the end, and (b) its 1R PRBM

This is a beam deflection issue. For large deflections, the beam deflection becomes nonlinear and is difficult to solve. Therefore, we adopted the pseudo-rigid-body model (PRBM) [21]. The PRBM uses a series of rigid body links and torsional springs to approximate a continuum beam. As shown in Fig. 4(a), the compliant tail is a continuum beam, having the pivot point O, and its deflection under force F is characterized by the angle θ_0. By contrast, Fig. 4(b) illustrates the 1R PRBM, which is characterized by three parameters: the radius factor, the stiffness coefficient, and the parametric angle coefficient. This 1R PRBM only approximates the tip position of the beam. For the compliant tail, the entire bending curve is crucial; hence, we must use multi PRBM. By following [28], we adopted the 3R PRBM, whose characteristic radius factors and stiffness coefficients are independent of the external loads. The 3R PRBM can accurately approximate very large deflections over a wide range of loading conditions.

Fig. 5 illustrates the design of the compliant tail and 3R PRBM. Unlike the existing 3R PRBM approximation issues, in which the loading is a point force or moment at the end [29-31], our robot fish swims in water, and hence, the external load of the compliant tail is a distributed hydrodynamic force (Fig. 3). This situation has been seldom studied before.

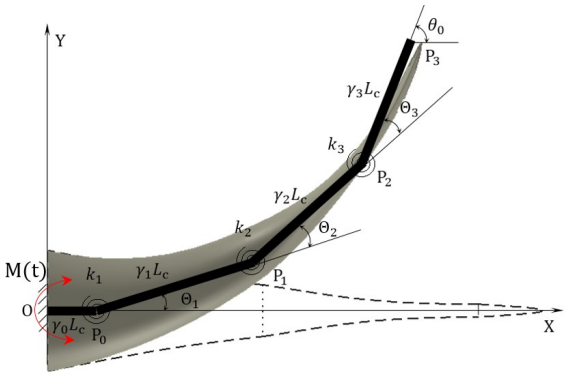

Figure 5. Modeling of the compliant tail

Our 3R PRBM is comprised of four rigid links jointed by pin joints and torsion springs. The characteristic radius factors γ_0, γ_1, γ_2, and γ_3 are the length ratios of the four rigid links and satisfy $\gamma_0 + \gamma_1 + \gamma_2 + \gamma_3 = 1$. k_1, k_2, and k_3 and θ_1, θ_2, and θ_3 denote the spring stiffness coefficients and deflection angles, respectively. The forward kinematics of this 3R PRBM can be represented as follows:

$$\begin{cases} P_{nx} = P_{(n-1)x} + \gamma_n L_c \cos\left(\sum_{i=0}^{n}\theta_i\right) \\ P_{ny} = P_{(n-1)y} + \gamma_n L_c \sin\left(\sum_{i=0}^{n}\theta_i\right) \end{cases}, \tag{9}$$

where $P_{ox} = \gamma_0 L_c$, $P_{oy} = 0$ and n = 1, 2, 3. By using this equation, the tip point of each link can be calculated.

Given the distributed hydrodynamic forces $L(x,t)$, the torques acting on each joint can be formulated as

$$\begin{cases} \tau_1 = k_1\theta_1 = \int_{\gamma_0 L_c}^{L_c} L(x,t)\left(x - \gamma_0 L_c\right)dx - M(t) \\ \tau_2 = k_2\theta_2 = \int_{(\gamma_0+\gamma_1)L_c}^{L_c} L(x,t)\left[x - (\gamma_0+\gamma_1)L_c\right]dx - M(t) \\ \tau_3 = k_3\theta_3 = \int_{(\gamma_0+\gamma_1+\gamma_2)L_c}^{L_c} L(x,t)\left[x - (\gamma_0+\gamma_1+\gamma_2)L_c\right]dx - M(t) \end{cases} \tag{10}$$

At time, t, the hydrodynamic forces have an exact distribution, and the moment $M(t)$ can be expressed as $M(t) = M_0 \sin(\omega t)$, where M_0 is the amplitude. From (10), the spring stiffness coefficients k_1, k_2, and k_3 can be calculated under the given deflection angles θ_1, θ_2, and θ_3, respectively. However, the deflection angles can only be found from the study of fish swimming.

According to Lighthill's model [32], the body curve of a fish swim can be modeled as follows:

$$h(x,t) = \left(c_1 x + c_2 x^2\right)\sin\left(kx + \omega t\right), \tag{11}$$

where c_1 is the linear wave amplitude envelope, c_2 is the quadratic wave amplitude envelope, k is the body wave number ($k = 2\pi/\lambda$, λ is the body wave length), and ω is the body wave frequency. The parameters in this model can be determined using the fish kinematics from the literature and considering a particular fish category, the exact body curve during swimming can be described. Once the body curve is confirmed in one moment, it can be matched using the 3R PRBM. For a given set of characteristic radius factors γ_0, γ_1, γ_2, and γ_3, the deflection angles θ_1, θ_2, and θ_3 can be determined by fitting the body curve of the fish swimming. Therefore, the spring stiffness coefficients k_1, k_2, and k_3 can be computed. In our design of the compliant tail, the material is the same (elasticity modulus); thus, the bending stiffness is determined by the cross section along the longitude direction. Therefore the spring stiffness coefficients k_1, k_2, and k_3 can be used to preliminarily design the profile of the compliant tail. The relationship from the bending stiffness to the spring stiffness [21] can be given by

$$k_n \approx \pi\gamma_n^{\,2}\frac{EI}{L_c} \tag{12}$$

In summary, the compliant tail design can be accomplished through (9) to (12). Following is the procedure:

- Step 1: Obtain a set of the characteristic radius factors γ_0, γ_1, γ_2, and γ_3 and use the 3R PRBM to match the body curve (11), and solve the inverse kinematics of (9) to obtain the deflection angles θ_1, θ_2, and θ_3.
- Step 2: Substitute the deflection angles θ_1, θ_2, and θ_3 and the distributed hydrodynamic forces $L(x,t)$ into (10) for computing the spring stiffness coefficients k_1, k_2, and k_3.
- Step 3: Based on the relationship between the bending stiffness EI and the spring stiffness in (12), the area moment of inertia I can be calculated to obtain the approximate geometry of the compliant tail.

III. Simulation and Model Analysis

In this section, we performed computer simulations to study the behavior of the ACPM. First, we assumed that the flapping of the active body follows a sinusoid pattern which was observed by biologists [33], that is, $\Phi(t) = A\sin(\omega t)$, where A is the amplitude and ω is the angular velocity. Fig. 6 displays the bending curves of the active body. In the figure, the flapping function is $\Phi(t) = 30\sin(2\pi t)$ and each curve represents the positions of the active body in $(1/8)^{th}$ of a cycle.

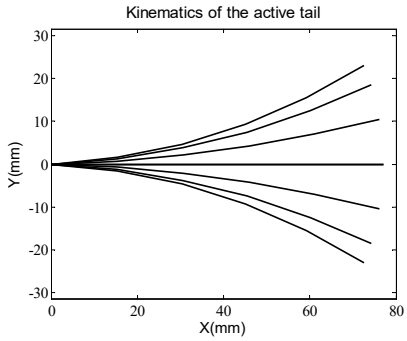

Figure 6. Flapping motion of the active body

Based on (4) and the designed parameters of the active part, the mapping relationship from active body bending angle Φ to motor rotation angle α is presented in Fig. 7.

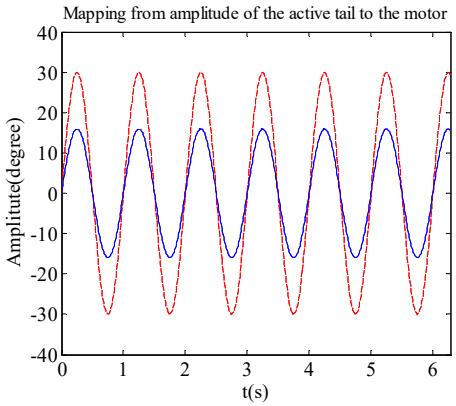

Figure 7. Mapping from the active body to the motor, the dashed red line is $\Phi(t)$ respect to time and the solid blue line is $\alpha(t)$ respest to time.

In this simulation, the amplitude of the active part is 30 degrees and its position changing principal is the function $\Phi(t)$. From Fig. 7, we can observe that the principal of the motor's motion is similar to that of the active part, except that its amplitude is nearly half of that of the active part.

To compute the bending curves of the compliant tail, we must obtain a relationship between the two coordinates systems: XOY and X'O'Y'. As shown in Fig. 3, the compliant tail starts at the end of the active part, and the coordinate system XOY is fixed on this end point. The position of this point can be formulated as follows:

$$\begin{cases} O_x = \sum_{i=1}^{N}\left(H+h\right)\cos\left(\dfrac{i\Phi}{N}\right) \\ O_y = \sum_{i=1}^{N}\left(H+h\right)\sin\left(\dfrac{i\Phi}{N}\right) \end{cases}, \tag{13}$$

where N is the number of vertebras and N=5. The homogeneous transformation matrix from the coordinate system XOY to the coordinate system X'O'Y' is given by

$$ {}^{O'}_{O}T = \begin{bmatrix} \cos\Phi & -\sin\Phi & O_x \\ \sin\Phi & \cos\Phi & O_y \\ 0 & 0 & 1 \end{bmatrix}. \quad (14) $$

By using this transformation matrix, the arbitrary point P_0 of the compliant tail in the coordinate system XOY can be expressed in the coordinate system X'O'Y' by

$$ P_{O'} = {}^{O'}_{O}TP_O . \quad (15) $$

Under a *sin* signal generator, we can simulate the body shape of the robot fish.

Under this driven signal of the motor, we can formulate the velocity distribution of the midline of the compliant tail. Obviously, the velocity of the midline is a linear distribution, and the velocity of the starting point O can be obtained from the time derivative of (13) and projection on the Y axis.

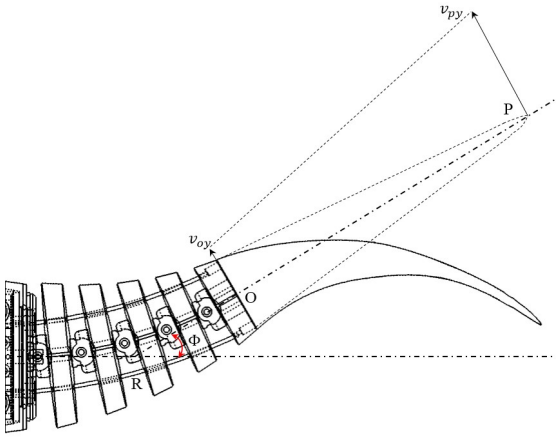

Figure 8. Velocity distribution caused by the movement of the active body

Fig. 8 depicts the velocity distribution before deflection (indicated by the dashed lines), which can be used to compute the distribution of the hydrodynamic forces, and then, under the hydrodynamic forces, we can predict the deflection of the compliant tail (indicated by the solid lines). First, the velocity of the starting point O is given by

$$ v_{oy} = \frac{1}{\cos\Phi}\frac{dO_y}{dt} = \frac{H+h}{5\cos\Phi}\sum_{i=1}^{5}\left(i\cos\left(\frac{i\Phi}{5}\right)\right)\frac{d\Phi}{dt}, \quad (16) $$

and then the velocity distribution of the midline at this moment (Fig. 8) is illustrated as a rod pivoted at point R and can be derived from the ratio between the distance from P to R and O to R, which is given by

$$ v_{py} = \frac{O_y + x\sin\Phi}{O_y} v_{oy}, x \in [0, L_c]. \quad (17) $$

From (6), (16) and (17), we computed the distribution of the hydrodynamic forces and further predicted the deflection of the compliant tail in coordinate system XOY, and obtained the midline position of the compliant tail by using (15). In the simulations, we assumed the slope $\partial h/\partial x$ to be the same along the longitude and equal to tan(Φ) for easily obtaining the hydrodynamic forces.

Fig. 9(a) presents the kinematics results of the ACPM under 1 Hz actuation frequency and 30 degrees amplitude of the active body, and shows the deflection of the compliant tail simplified using the 3R PRBM under distributed hydrodynamic forces. In this simulation, the series values of the characteristic radius factors, respectively, are $\gamma_0 = 0.1$, $\gamma_1 = 0.35$, $\gamma_2 = 0.4$, and $\gamma_3 = 0.15$ based on the optimal values in [29].The black solid lines denote the body curve of the active part from 0 to T divided with $T/8$, and the blue dashed lines denote the body curve of the compliant tail. The blue points in the active part curve are the joints between every two vertebras, and the last four blue points on every blue dashed line denote P_0, P_1, P_2, and P_3, respectively corresponding to that in Fig. 5.

The result clearly indicates the deflection of every joint of the rigid links. To compare these results with the midline curves of the real compliant tail, B-spline curves (red solid lines) were used to fit the body curve of the compliant tail, replacing the four rigid links in the 3R PRBM (Fig. 9(b)). In the next section, these simulation results based on the 3R PRBM system model are verified using the experimental results.

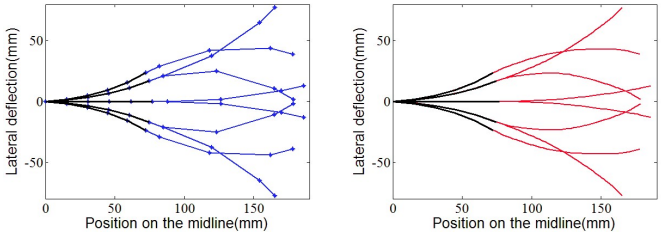

Figure 9. Kinematics of the ACPM: (a) simulation results and (b) midline curves fitted using B-spline curves

IV. Prototype and Experiments

A. Prototype and Fabrication

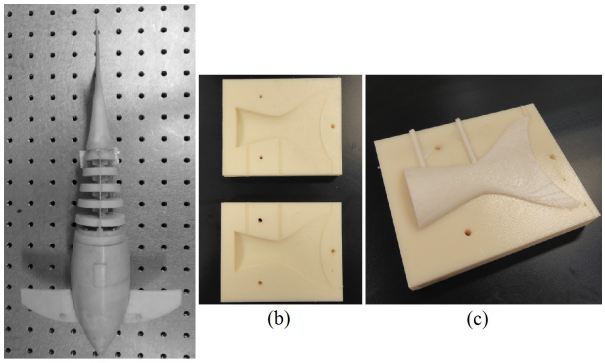

Figure 10. (a) is the propotype of the robot fish, (b) is the mold and (c) is the fabricated compliant tail

Fig. 10(a) depicts the prototype of the robot fish having a length of 310 mm, in which the active body is 77 mm and the compliant tail is 110 mm. These dimensions are based on the study of the subcarangiform swimming fish described in [16]. The rigid body is approximately 40% ((310 – 77 – 110)/310 = 0.39) of the total length and the length involved in flapping (including the active and the compliant tails) is approximately 60%. A steel wire of Φ0.5 mm is used to drive the active body. A

set of pectoral fins is used to achieve the ascending and descending motions (though, its function are not detailed in this study).

The head hosts all electronic and mechanical parts, including an Arduino Nano control board, KST (KST Digital Technology Ltd.) DS1509MG motor and driver, and APC220 radio communication module for remote control. The total weight of the robot fish is nearly 0.5 kg, and lead beads are used for adjusting the center of gravity.

The fabrication of the prototype is straightforward. The structural parts were constructed by 3D printing, including the shell of the head, vertebras of the active body, and the reel. The design parameters of the active body are presented in Table 1. The compliant tail is composed of silicon rubber and is fabricated by casting. Its material properties are presented in Table 1.

TABLE 1 DIMENSIONS AND PROPERTIES OF THE MECHANISM

The dimensions of the active body	
H	8.4 mm
h	7 mm
d	24 mm
L_a	77 mm
The material properties of the compliant tail	
E	80 KPa
ρ	1080 kg/m^3

Fig. 10(b) exhibits the mold made by 3D printing and Fig. 10(c) displays the fabricated complaint tail. Finally, the compliant tail is mounted on the last vertebra of the active body, and the active body is covered by silica gel skin for water proofing.

B. Kinematics Testing

To test the kinematics of the ACPM and verify the proposed design methodology of the compliant tail, we captured a series video frames of the robot fish in air and in water. In all tests, the rigid head was stationary. When testing the robot fish in water, silica gel skin of 0.03 mm thickness was used for waterproof, and because of its excellent elasticity, its influence on the accuracy of kinematics can be ignored. Fig. 11 depicts the experimental results of tail flapping of the robot fish in air and in water, which are evaluated by analyzing the video frames. The experiments done in air were just for comparison. In each flapping cycle, T, eight frames were captured with identical interval.

The left-side column in Fig. 11 shows the experimental results in air, in which the flapping amplitude of the active body is 30 degrees and the flapping frequency is 1 Hz. In each frame, the dashed red line denotes the model-based predicted flapping curves, and the solid blue line denotes the experimental result. From these curves, we can observe that the compliant tail bends little during flapping motion, and the actual flapping curves are quite different from those of prediction. This is because air provides little resistance to the complaint tail, and under this condition, the ACPM cannot perform a perfect 'S' shape motion.

The right-side column in Fig. 11 shows the experimental results in water with the same flapping amplitude and flapping frequency. The dashed red line is the same as that of the left column, and the blue lines are the experimental results. From these curves, we can observe that the two curves are similar. The compliant tail bends a lot under the hydrodynamic forces, and together with the active body, it can perform a perfect 'S' shape motion.

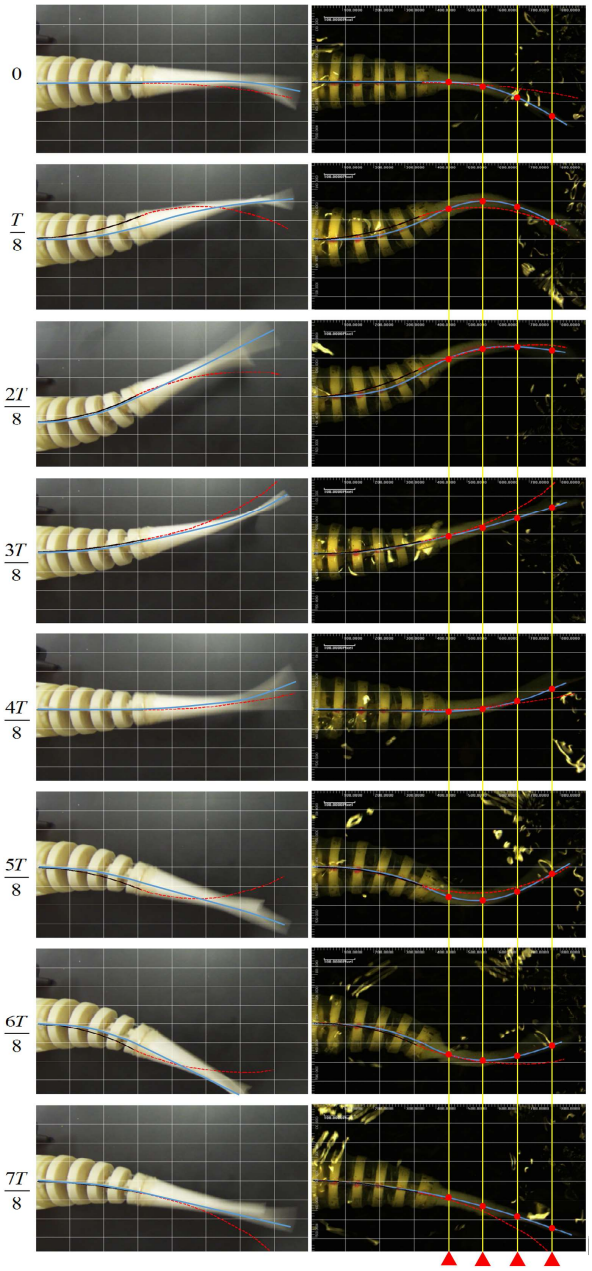

Figure 11. Experiment results in one flapping circle: the left-side column displays the results in air, and the right-side column displays the results in water.

To measure and analyze the errors between experimental flapping curves and model predicted flapping curves, each frame was divided into 64 small rectangles for easy of measurement and the dimension of each rectangle was 25 × 15 mm. Moreover, a MATLAB ® program was developed for computing the flapping curves (i.e., the midline curves of the flapping tail). Four markers, which intersected with four longitudes in video frame, were related to the compliant tail. Through measuring the

distances between the markers and the intersections of the four longitudes and predicted curves, we obtained the errors. Fig. 12 depicts the errors of the compliant tail curves between the experimental results and the model-based prediction, in which each curve represents 1/8 of a flapping cycle, and the points on each curve are errors of the four markers on the compliant tail. The maximum error is 18 mm, which appears at the last marker of the compliant tail; considering the length of the ACPM is 187 mm, the error is about 18/187 ≈ 9.6%. The discrepancy may be attributed to a number of factors. The main factor is the shape of the caudal fin, in the design and modelling, we treat caudal fin as part of the compliant tail and neglect the shape of it.

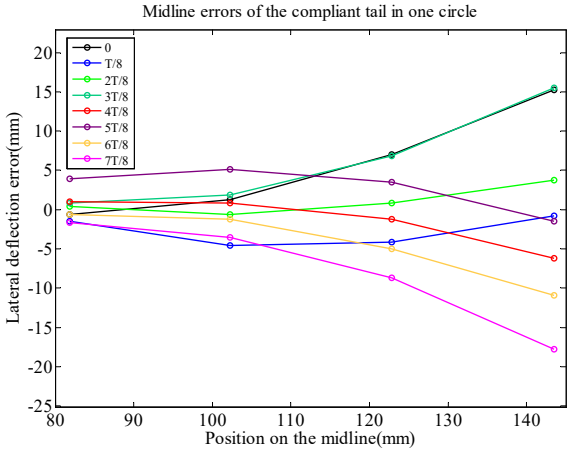

Figure 12. Midline deflection errors compared to the prediction.

These results demonstrate that the midline curves of the tail match with the predicted curves much better in water than that in air and the kinematics can be predicted using the proposed methodology. The hydrodynamic forces greatly influence the deflection of the compliant tail, and the ACPM can perform the "S" shape motion in water.

C. *Swimming Performance*

Our robot fish can perform multi-modal motion, including swimming forward, turning motion (escape motion), ascending and descending motions. In this study, we mainly addressed on swimming speed of the forward motion and turning performance.

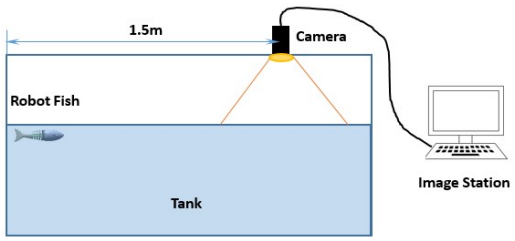

Figure 13. Experiment setup

The first experiment was to test swimming speed of the robot fish, a 2m×1m×1.2m tank was set up with an industrial camera above (Fig. 13). The camera was install at the 1.5m length position of the tank and the robot fish started swimming from the left side of the tank. After 1.5m swimming distance, the robot fish was captured by the camera with 240 frames per second speed. Swimming speeds were obtained by analyzing the position changes in the video frames. During experiments, unless otherwise stated, the data points and error bars shown in subsequent figures were the averages and standard deviations of two runs. Fig. 14 shows the results:

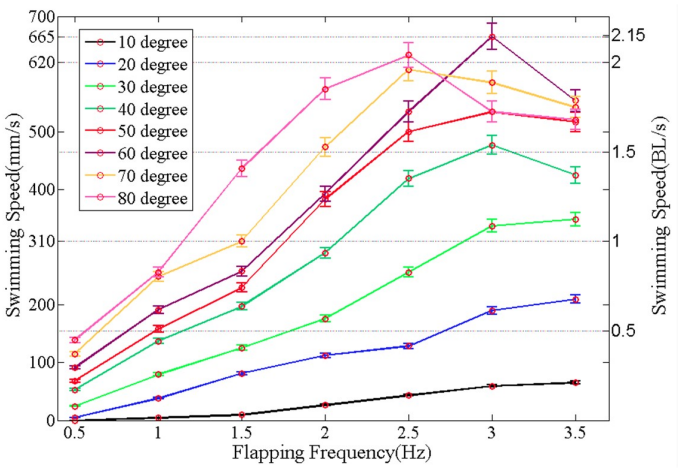

Figure 14. The swimming speed with respect to flapping frequency and amplitude. The flapping amplitude is bending angle Φ of the active body, the setting values are 10°, 20°, 30°, 40°, 50°, 60°, 70°, and 80°, repectively.

The swimming speed evidently increased with the increases of flapping frequency and amplitude. Regarding to the relationship between swimming speed and flapping frequency, the data depicts that the swimming speed increased linearly to flapping frequency till the motor peaked its respond speed limit. In concrete terms, below 2.5 Hz, it maintains linear relationship; over 2.5 Hz flapping frequency and 60 degrees flapping amplitude, the growth of swimming speed became slow and even the speed started to decrease at 60 degrees amplitude.

To compare the performance with other robot fish, length-specific speed expressed as body length per second (BL/s) is applied. Remarkably, the maximum speed of our robot fish could reach 2.15 BL/s obtained at 3 Hz flapping frequency and 60 degrees amplitude. From the literature, the swimming speed of most robot fish peaked 1BL/s. For example, Anderson's robotic tuna achieved a maximum speed of 0.6 BL/s (1.2 m/s) [34], Yu's carangiform swimmer achieved a maximum speed of 0.8 BL/s (0.32m/s) [35], Wen's carangiform swimmer achieved a maximum speed of 0.98 BL/s [36], Essex's G9 achieved a maximum speed of 1.02 BL/s (0.5 m/s) [37], Valdivia y Alvarado's compliant method achieved a maximum speed of 1.1 BL/s (0.32 m/s) [38], and Hu's iSplash robot fish achieved a maximum speed of 11.6 BL/s with a frequency of 20Hz [39](but this robot fish was designed only for straight line swimming and could not achieve any other maneuverable motions).

From the comparison, it can be concluded that compared with the existing robot fish which are capable of multi-modal swimming motions (the iSplash does not belong to this category), the swimming speed of our robot fish reached the top list.

The second experiment is to test turning performance of the robot fish. A series of video frames (Fig. 15) displays a typical turning motion: in every turning motion circle, the robot fish first rapidly flaps its tail to the limit position defined as *beat phase*

(this position is determined by the mechanical structure and program setting), and then restore to the initial position slowly defined as *restore phase*. β is the turning angle of each turning circle. During the beat phase, the active body bends in a 'C' shape, while the compliant tail is driven to bending in opposite orientation, forming an 'S' shape. When the active body reach the limit position, the compliant tail subsequently restore to the initial state (no bending) [40]; at this moment, the robot fish reaches the maximum bending angle (Fig. 15A-D). In the restore phase, the active body restore to the initial state, followed by the compliant tail (Fig. 15D-F).

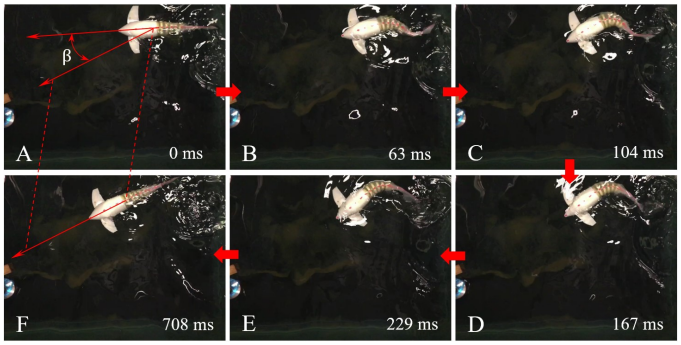

Figure 15. Sequences depicting the turning motion in one circle. Each circle contains a beat phase (A-D) and a restore phase (D-F). The maximum tunring angle is obtained at the end of beat phase and in the restore phase the turning angle decreases a little.

In our experiments, we tested different beating angles of the beat phase and different time ratio between beat phase and restore phase to explore superior turning performance (not detailed in this paper). In our findings, the robot fish reached a maximum turning angle of 45 degrees at approximately 167 ms obtained at the end of beat phase, achieving a maximum turning speed of 269 degrees per second; and in each turning circle, it could turn 38 degrees in approximately 708 ms (depicted in Fig. 15A and F), achieving an average turning speed of 54 degrees per second.

These results displaye a good maneuverability of our robot fish (a free swimming video can be view through the link[1]). It can swim forward at a relatively high speed and simultaneously achieve quick and effective turning motion. To assess the performance of the robot fish, we examined the Strouhal number, Reynolds number and Froude efficiency under the maximum swimming speed (i.e., the flapping frequency is 3 Hz and flapping amplitude is 60 degree). The Strouhal number is about 0.39, the Reynolds number is nearly 2.1×10^5, and the Foude efficiency based on the elongated body theory is about 0.86.

V. Conclusions

This paper presents a novel robot fish that can achieve subcarangiform swimming (undulatory motion) by using just one motor. Based on the earlier discussions, the following conclusions can be derived:

- The design methodology of our robot fish, refer in particular to the compliant tail, is experimentally proved to be effective. Moreover, the active body can be modeled using simple kinematics. The complaint tail can be modeled approximated by the 3R PRBM.
- The new robot fish swam extremely well. It achieved a maximum speed of 2.15 BL/s and a maximum average turning speed of 63°/s.
- In addition, the proposed methodology also can be used to preliminarily design the soft compliant parts in other biomimetic robots, soft manipulators, and other applications.

[1] Website: https://www.youtube.com/watch?v=RPjFQtVar7k

References

[1] Wen L, Wang T, Wu G, et al. "Novel method for the modeling and control investigation of efficient swimming for robotic fish". *Industrial Electronics, IEEE Transactions on*, 2012, 59(8): 3176-3188.

[2] J. Yu, M. Tan, S. Wang, and E. Chen, "Development of a biomimetic robotic fish and its control algorithm," *Systems, Man, and Cybernetics, Part B: Cybernetics, IEEE Transactions on*, vol. 34, pp. 1798-1810, 2004.

[3] Ren Q, Xu J, Yang S, et al. "Design and implementation of a biomimetic robotic fish with 3D locomotion", *Control & Automation (ICCA), 11th IEEE International Conference on. IEEE*, 2014: 139-144.

[4] Jia Y, Wang L. "Experimental implementation of distributed flocking algorithm for multiple robotic fish". *Control Engineering Practice*, 2014, 30: 1-11.

[5] Triantafyllou M S, Triantafyllou G S, Yue D K P. "Hydrodynamics of fishlike swimming". *Annual review of fluid mechanics*, 2000, 32(1): 33-53.

[6] Wang Z, Hang G, Wang Y, et al. "Embedded SMA wire actuated biomimetic fin: a module for biomimetic underwater propulsion". *Smart Materials and Structures*, 2008, 17(2): 025039.

[7] Low K H, Yang J, Pattathil A P, et al. "Initial prototype design and investigation of an undulating body by SMA", *Automation Science and Engineering, 2006. CASE'06. IEEE International Conference on. IEEE*, 2006: 472-477.

[8] Chen Z, Shatara S, Tan X. "Modeling of biomimetic robotic fish propelled by an ionic polymer–metal composite caudal fin". *Mechatronics, IEEE/ASME Transactions on*, 2010, 15(3): 448-459.

[9] Tan X, Kim D, Usher N, et al. "An autonomous robotic fish for mobile sensing". *Intelligent Robots and Systems, 2006 IEEE/RSJ International Conference on. IEEE*, 2006: 5424-5429.

[10] P. V. y. Alvarado, "Design of Biomimetic Compliant Devices for Locomotion in Liquid Environments," MIT PhD Thesis, 2007.

[11] B. P. Epps, P. Valdivia y Alvarado, K. Youcef-Toumi, and A. H. Techet, "Swimming performance of a biomimetic compliant fish-like robot," *Experiments in Fluids,* vol. 47, pp. 927-939, 2009.

[12] Fiazza, C., et al. "Biomimetic mechanical design for soft-bodied underwater vehicles." *OCEANS 2010 IEEE-Sydney*. IEEE, 2010.

[13] H. El Daou, T. Salumae, L. D. Chambers, W. M. Megill, and M. Kruusmaa, "Modelling of a biologically inspired robotic fish driven by compliant tails," *Bioinspir Biomim,* vol. 9, p. 016010, Mar 2014.

[14] K. L. Feilich and G. V. Lauder, "Passive mechanical models of fish caudal fins: effects of shape and stiffness on self-propulsion," *Bioinspir Biomim,* vol. 10, p. 036002, 2015.

[15] Kopman V, Laut J, Acquaviva F, et al. "Dynamic modeling of a robotic fish propelled by a compliant tail". *Oceanic Engineering, IEEE Journal of,* 2015, 40(1): 209-221.

[16] D. M. L. Michael Sfakiotakis, and J. Bruce C. Davies, "review of fish swimming modes for aquatic locomotion," *IEEE JOURNAL OF OCEANIC ENGINEERING,* vol. 24(2), pp. 237-252, 1999.

[17] Lee K. "Large deflection of viscoelastic fiber beams". *Textile Research Journal,* 2007, 77(1): 47-51.

[18] Bisshopp K E, Drucker D C. "Large deflection of cantilever beams". *Quarterly of Applied Mathematics,* 1945, 3(1).

[19] Haslach H W. "Post-buckling behavior of columns with non-linear constitutive equations". *International journal of non-linear mechanics,* 1985, 20(1): 53-67.

[20] Yin Y Z, Wang Y C. "A numerical study of large deflection behaviour of restrained steel beams at elevated temperatures". *Journal of Constructional Steel Research,* 2004, 60(7): 1029-1047.
[21] L. L. Howell, Compliant mechanisms: John Wiley & Sons, 2001.
[22] Yu Y Q, Howell L L, Lusk C, et al. "Dynamic modeling of compliant mechanisms based on the pseudo-rigid-body model". *Journal of Mechanical Design*, 2005, 127(4): 760-765.
[23] Z. Li and R. Du, "Design and analysis of a bio-inspired wire-driven multi-section flexible robot," *Int J Adv Robotic Sy,* vol. 10, 2013.
[24] Y. Zhong, Z. Li and R. Du, "The design and prototyping of a wire-driven robot fish with pectoral fins," *Robotics and Biomimetics (ROBIO), 2013 IEEE International Conference on. IEEE,* 2013.
[25] B. Liao, Z. Li, and R. Du, "Robot fish with a novel biomimetic wire-driven flapping propulsor," *Advanced Robotics,* vol. 28, pp. 339-349, 2014.
[26] Ruxu Du, Zheng Li, Kamal Youcef-Toumi and Pablo Valdivia y Alvarado, ed., Robot Fish, Bio-Inspired Fishlike Underwater Robots, Springer, 2015.
[27] T. Y. Wu, "Mathematical biofluiddynamics and mechanophysiology of fish locomotion," *Mathematical Methods in the Applied Sciences,* vol. 24, pp. 1541-1564, 2001.
[28] H.-J. Su, "A pseudorigid-body 3R model for determining large deflection of cantilever beams subject to tip loads," *Journal of Mechanisms and Robotics,* vol. 1, p. 021008, 2009.
[29] H.-J. Su, "A load independent pseudo-rigid-body 3r model for determining large deflection of beams in compliant mechanisms," *Proceedings of ASME IDETC/CIE (43260),* pp. 109-121, 2008.
[30] G. Chen, B. Xiong, and X. Huang, "Finding the optimal characteristic parameters for 3R pseudo-rigid-body model using an improved particle swarm optimizer," *Precision Engineering,* vol. 35, pp. 505-511, 2011.
[31] Khoshnam M, Patel R V. "A pseudo-rigid-body 3R model for a steerable ablation catheter", *Robotics and Automation (ICRA), 2013 IEEE International Conference on. IEEE, 2013*: 4427-4432.
[32] Lighthill M J. "Large-amplitude elongated-body theory of fish locomotion". *Proceedings of the Royal Society of London B: Biological Sciences*, 1971, 179(1055): 125-138.
[33] Čech M, Kubečka J. "Sinusoidal cycling swimming pattern of reservoir fishes". *Journal of Fish Biology,* 2002, 61(2): 456-471.
[34] Anderson J M, Chhabra N K. "Maneuvering and stability performance of a robotic tuna". *Integrative and comparative biology*, 2002, 42(1): 118-126.
[35] Yu J, Tan M, Wang S, et al. "Development of a biomimetic robotic fish and its control algorithm". *Systems, Man, and Cybernetics, Part B: Cybernetics, IEEE Transactions on*, 2004, 34(4): 1798-1810.
[36] Wen L, Wu G, Li J. "Hydrodynamic experimental investigation on efficient swimming of robotic fish using self-propelled method". *International Journal of Offshore and Polar Engineering*, 2010, 20(03).
[37] Liu J, Hu H. "Biological inspiration: from carangiform fish to multi-joint robotic fish". *Journal of Bionic Engineering*, 2010, 7(1): 35-48.
[38] y Alvarado P V, Youcef-Toumi K. "Modeling and Design Methodology of an Efficient Underwater Propulsion System". *Robotics and Applications.* 2003: 161-166.
[39] Clapham R J, Hu H. "iSplash: Realizing Fast Carangiform Swimming to Outperform a Real Fish". *Robot Fish. Springer Berlin Heidelberg,* 2015: 193-218.
[40] HARPER D G, BLAKE R W. "Fast-start performance of rainbow trout Salmo gairdneri and northern pike Esox lucius". *Journal of Experimental Biology*, 1990, 150(1): 321-342.